Thermal Stability and Degradation Studies of Alternating Poly(ester amide)s Derived from Glycolic Acid and ω-Amino Acids

E. Botines, L. Franco, J. Puiggalí

Departament d'Enginyeria Química, Universitat Politècnica de Catalunya, Av. Diagonal 647, E-08028, Barcelona, Spain.

Received 15 February 2006; accepted 28 April 2006
DOI 10.1002/app.24725
Published online in Wiley InterScience (www.interscience.wiley.com).

ABSTRACT: The thermal degradation of three poly(ester amide)s derived from glycolic acid and different ω-amino acids is studied by thermogravimetric analysis (TGA) at different heating rates and the results are compared. Thermal decomposition follows a two-step reaction, the mechanism involved in each step being possible to be determined. Non-isothermal integral isoconversional methods (such as Kissinger, KAS, and Flynn–Wall–Ozawa) and linear equations and differential methods (such as the Friedman expression) were used to obtain the kinetic parameters from TGA and DTGA curves. The complete kinetic triplets are also determined by the Coats–Redfern and the invariant kinetic parameters methodologies. Hydrolytic and enzymatic degradation studies, where weight losses, intrinsic viscosity changes and NMR spectra of degraded samples are evaluated, are also undertaken. The polymers seem interesting because of their application as new biodegradable materials. © 2006 Wiley Periodicals, Inc. J Appl Polym Sci 102: 5545–5558, 2006

Key words: glycolic acid derivatives; bioabsorbable sutures; degradability; kinetic parameters

INTRODUCTION

Considerable effort is now focused on the preparation of biodegradable materials that may be useful for biomedical applications. Bioabsorbable surgical sutures constitute an example of this kind of specialized polymers. A combination of different properties, which is difficult to obtain (e.g., flexibility, high tensile strength, nontoxicity of degradation products or fitting between the degradation rate, and the temporary function), is required.[1,2] Thus, new materials, which are mainly based on changes both in composition and chain microstructure (i.e., random or block distribution) are continuously being developed. Ring opening polymerization of monomers like glycolide, lactide, caprolactone, trimethylcarbonate, and 1,4-dioxan-2-one has rendered the most bioabsorbable surgical sutures so far commercialized, which consist of homopolymers (e.g., polyglycolide[3] (Dexon®, Safil®) and poly(*p*-dioxanone)[4] (PDS®, Monoplus®)) and copolymers of the above monomers (e.g., poly(glycolide-*co*-lactide)[5] (Vicryl®), poly(glycolide-*co*-caprolactone)[6] (Monocryl®), and poly(glycolide-*co*-trimethylenecarbonate)[7] (Maxon®)).

Correspondence to: J. Puiggalí (Jordi.Puiggali@upc.es).
Contract grant sponsor: CICYT and FEDER; contract grant number: MAT2003-01,004.

Poly(ester amide)s have been the object of extensive research during the last few decades since the presence of amide and ester groups may render a combination of the characteristic properties of polyamides (heat stability and high tensile strength) and polyesters (high degradability and flexibility). These new materials appear interesting for environmental (e.g., BAK[8]) and biomedical applications. Several types of poly(ester amide)s have been synthesized and characterized,[9–16] which can be prepared with a blocky nature or with a well-defined sequence like the derivatives of alcohol amines and dicarboxylic acids,[17–19] or the derivatives of amino acids, diols, and dicarboxylic acids.[20–22]

Furthermore, some poly(ester amide)s have been patented as bioabsorbable surgical sutures.[23,24] These were obtained by the reaction of a diamidediol and a dichloride of a dicarboxylic acid and were defined by the repeat unit —[OCH_2CO—$NH(CH_2)_nNH$—$COCH_2O$—$CO(CH_2)_{m-2}CO$]— (group I). Polymers with an alternate disposition of an α-hydroxyacid and an ω-amino acid (—[OCR_2CO—$NH(CH_2)_{n-1}CO$] —, group II) have also been patented as surgical devices.[25,26] In this case, the synthesis is more complex since it requires the preparation of a cyclic monomer that contains both units. The particular case of glycolic acid and α-amino acid derivatives corresponds to the well-known polymerization of morpholine-2,5-diones.[27,28]

We have recently found that polymers of the two aforementioned groups can be easily synthesized with high yields and relatively high molecular weights by a

new thermal polycondensation method that involves the formation of metal halide salts as a driving force.[29] These results again raise interest in the properties and the applicability of the indicated poly(ester amide)s. Polymerization kinetics have been studied for some samples[30] and the degradability of polymers corresponding to the first group has been evaluated.[31]

In this work, the stability of three samples with a different methylene content that belong to the second group of polymers is comparatively studied and the molecular mechanism involved in the thermal degradation is investigated. Furthermore, hydrolytic and enzymatic degradabilities are evaluated. These samples are referred to by the acronym PEA(glc-*n*), where the PEA refers to poly(ester amide) and the digit *n* indicates the number of carbon atoms of the ω-amino acid.

Thermal stability is a crucial factor to determine the processing and application of materials. The thermal degradation kinetics of some products commercialized as surgical sutures has recently been studied (e.g., poly(*p*-dioxanone)[32]), but the available information on glycolide derivatives is scarce. Previous calorimetric data performed with alternate copolymers constituted by glycolic acid units and different amino acids showed that thermal degradation takes place in two steps.[31]

EXPERIMENTAL

Materials

Poly(ester amide)s were synthesized following a previously reported method,[29] based on a thermal polycondensation with formation of metal halide salts as a driving force (Scheme 1). The synthesis and characterization of the studied polymers had been previously described.[29,33,34] The samples used in this work had melting points of 157°C (PEA(glc-6)), 123°C (PEA(glc-11)), and 128°C (PEA(glc-12)). The intrinsic viscosities of the samples employed in the thermal analyses were 0.75 dL/g (PEA(glc-6)), 1.0 dL/g (PEA(glc-11)), and 0.85 dL/g (PEA(glc-12)) (measured at 25°C using dichloroacetic acid as a solvent). To point out that polymers with a higher methylene content in the repeat unit degrade at a lower rate, samples of PEA(glc-11) with a lower molecular weight ([η] of 0.55 dL/g) were used in hydrolytic and enzymatic degradation studies.

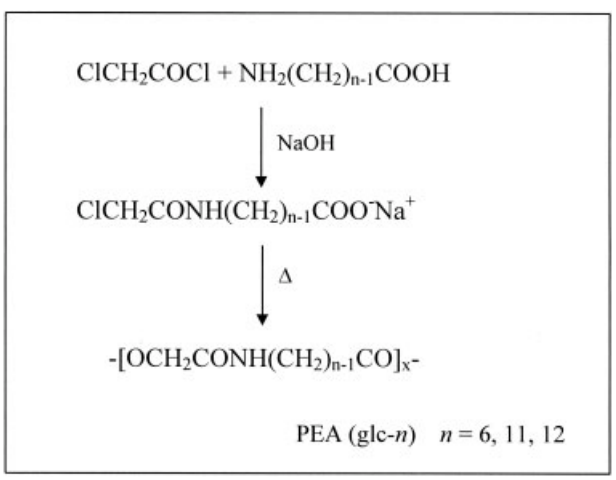

Scheme 1

Measurements

Infrared absorption spectra were recorded on a Perkin–Elmer 1600 FTIR spectrometer in the 4000–500 cm^{-1} range from films obtained by evaporation of trifluoroacetic solutions. NMR spectra were obtained with a Bruker AMX-300 spectrometer operating at 300.1 MHz for ^1H NMR investigations. Chemical displacements were calibrated using tetramethylsilane as an internal standard. Intrinsic viscosities were measured with a Cannon-Ubbelhode microviscometer in dichloroacetic acid solutions at 25 ± 0.1°C.

Thermogravimetric analyses (TGA) were performed at heating rates ranging from 2 to 40°C/min using a Perkin–Elmer TGA-6 thermobalance under a flow of dry nitrogen, some experiments were also carried out in an oxidative air atmosphere. The sizes of TGA samples ranged from 5 to 10 mg for these studies.

Deconvolution of the derivative thermogravimetric analysis (DTGA) curve was performed with the Peak.-fit program by Jandel Scientific Software, using a mathematical function known as ''asymmetric double sigmoidal.''

The plate samples (15 mm × 15 mm) for the degradation studies were cut off from regular films of 200 mm in thickness prepared by melt pressing 200 mg of the appropriate polymer at a temperature of 10°C below the melting peak temperature.

Hydrolytic degradation assays were carried out in phosphate buffer (pH 7.4) at 37°C and under accelerated conditions using distilled water at 70°C, or sodium citrate buffer (pH 2.3) at 37°C. Each plate was kept in a bottle filled with 30 mL of the medium and sodium azide (0.03 wt %) to prevent microbial growth. After the immersion time, the retrieved samples were thoroughly rinsed with distilled water. The remaining samples were dried to constant weight under vacuum and stored over $CaCl_2$ before analysis.

Enzymatic degradation was also studied and conducted at 37°C using a lipase from *Pseudomonas cepacia* (LPC) and proteinase K as a proteolytic enzyme. The enzymatic medium, 10 mL, consisted of sodium phosphate buffer solution (pH 7.4) containing sodium azide (0.03 wt %) and 1 mg of the appropriate enzyme. All enzymatic solutions were renewed every 72 h because of enzymatic activity loss. After the immersion time, the retrieved samples were immersed in HCl solution, rinsed with water, and dried as indicated for hydrolytic experiments.

Mass loss, intrinsic viscosity, and changes in NMR spectra were evaluated in these hydrolytic and enzymatic degradation studies. Scanning electron microscopy was used to examine the changes in the texture of samples after degradation. Gold coating was accomplished by using a Balzers SCD-004 Sputter Coater. SEM micrographs were obtained with a JEOL JSM-6400 instrument.

Kinetics methods

In thermogravimetric analysis, the rate of degradation, $d\alpha/dt$, can be defined as the variation in the degree of conversion, α, with time. The degree of degradation or conversion is calculated in terms of mass loss as

$$\alpha = \frac{W_0 - W}{W_0 - W_\infty} \tag{1}$$

where W_0, W, and W_∞ are the initial weight, the actual weight at each point of the curve, and the final weight at the end of the degradation process, respectively.

According to nonisothermal kinetic theory, the thermal degradation of a polymer can also be expressed as the variation in the degree of conversion with temperature by the following function:

$$\frac{d\alpha}{dT} = \frac{1}{\beta} A \exp\left(\frac{-E}{RT}\right) f(\alpha) \tag{2}$$

where $f(\alpha)$ is the differential conversion function, β is the heating rate, T is the absolute temperature, R is the gas constant, A and E are the preexponential factor and the activation energy for the decomposition reaction, respectively.

The integration of the rate equation (2) leads to

$$g(\alpha) = \int_0^\alpha \frac{d\alpha}{f(\alpha)} = \frac{A}{\beta} \int_0^T e^{-E/RT}\, dT \tag{3}$$

The differential ($f(\alpha)$) and the integral ($g(\alpha)$) conversion functions, summarized in Table I, can take different forms[35] according to the reaction mechanism.

The most probable mechanism can be determined by using the Coats–Redfern approximation[36] to solve eq. (3) and considering that $2RT/E \ll 1$, this equation may be rewritten as

$$\ln \frac{g(\alpha)}{T^2} = \ln\left(\frac{AR}{\beta E}\right) - \frac{E}{RT} \tag{4}$$

For a given kinetic model, the linear representation of $\ln[g(\alpha)/T^2]$ versus $1/T$ makes it possible to determine E and A from the slope and the ordinate at the origin. The model can be selected taking into account the linear regression coefficient (r) and the agreement of the activation energy with that estimated by the isoconversional methods as will be explained.

Thus, by reordering eq. (4), we can write

$$\ln \frac{\beta}{T^2} = \ln\left[\frac{AR}{g(\alpha)E}\right] - \frac{E}{RT} \tag{5}$$

The linear representation of $\ln(\beta/T^2)$ versus $1/T$ allows E to be determined for every degree of conversion, which is the basis of the KAS isoconversional method.[37]

Other methods such as those of Friedman,[38] Kissinger,[37] and Flynn–Wall–Ozawa[39,40] were also used in the literature to determine the activation energy.

The Friedman equation results from the logarithmic form of the rate equation (2):

$$\ln\left(\beta \frac{d\alpha}{dT}\right) = \ln A + \ln f(\alpha) - \frac{E}{RT} \tag{6}$$

For α = constant, the plot of $\ln [\beta\, d\alpha/dT]$ versus $1/T$, obtained from thermograms recorded at several heat-

TABLE I
Algebraic Expressions of $f(\alpha)$ and $g(\alpha)$ for the Kinetics Models Considered in This Work

Symbol	Reaction model	$f(\alpha)$	$g(\alpha)$
$A_{3/2}$	Avrami–Erofeev equation ($n = 1.5$)	$3/2(1-\alpha)[-\ln(1-\alpha)]^{1/3}$	$[-\ln(1-\alpha)]^{2/3}$
A_2	Avrami–Erofeev equation ($n = 2$)	$2(1-\alpha)[-\ln(1-\alpha)]^{1/2}$	$[-\ln(1-\alpha)]^{1/2}$
A_3	Avrami–Erofeev equation ($n = 3$)	$3(1-\alpha)[-\ln(1-\alpha)]^{2/3}$	$[-\ln(1-\alpha)]^{1/3}$
A_4	Avrami–Erofeev equation ($n = 4$)	$4(1-\alpha)[-\ln(1-\alpha)]^{3/4}$	$[-\ln(1-\alpha)]^{1/4}$
D_1	One-dimensional diffusion or parabolic law	$(2\alpha)^{-1}$	α^2
D_2	Two-dimensional diffusion (Valensi equation)	$-\ln(1-\alpha)^{-1}$	$(1-\alpha)\ln(1-\alpha) + \alpha$
D_3	Three-dimensional diffusion (Jander equation)	$3/2(1-\alpha)^{2/3}[1-(1-\alpha)^{1/3}]^{-1}$	$[1-(1-\alpha)^{1/3}]^2$
D_4	Three-dimensional diffusion (Ginstling–Brounshtein equation)	$3/2(1-\alpha)^{1/3}[1-(1-\alpha)^{1/3}]^{-1}$	$1 - 2/3\alpha - (1-\alpha)^{2/3}$
R_2	Contracting area (cylindrical symmetry)	$2(1-\alpha)^{1/2}$	$1-(1-\alpha)^{1/2}$
R_3	Contracting volume (spherical symmetry)	$3(1-\alpha)^{2/3}$	$1-(1-\alpha)^{1/3}$
$n + m = 2$; n=1.5	Autocatalytic reaction	$(\alpha)^{0.5}(1-\alpha)^{1.5}$	$[(1-\alpha)\alpha^{-1}]^{-0.5}(0.5)^{-1}$
$n + m = 2$; n=1.9	Autocatalytic reaction	$(\alpha)^{0.1}(1-\alpha)^{1.9}$	$[(1-\alpha)\alpha^{-1}]^{-0.9}(0.9)^{-1}$
$n = 2$	Second-order	$(1-\alpha)^2$	$-1+(1-\alpha)^{-1}$
$n = 3$	Third-order	$(1-\alpha)^3$	$2^{-1}[-1+(1-\alpha)^{-2}]$
F_1 or n=1	Random nucleation or first order kinetics	$(1-\alpha)$	$-\ln(1-\alpha)$
Power	Power law	$2(\alpha)^{1/2}$	$(\alpha)^{1/2}$

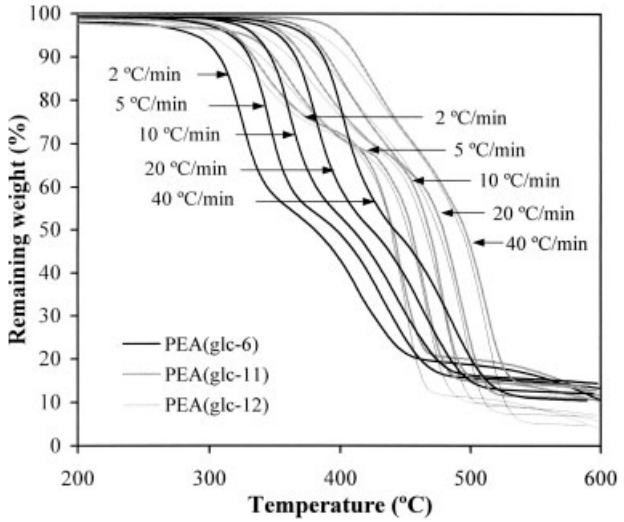

Figure 1 Thermogravimetric curves of PEA (glc-*n*) samples at different heating rates.

ing rates, should be a straight line whose slope allows an evaluation of the activation energy.

The Kissinger equation can be considered a particular case of eq. (5) applied for $\alpha = \alpha_{max}$ (the conversion at maximum weight loss rate) and assuming $f(\alpha) = (1 - \alpha)^n$:

$$\ln \frac{\beta}{T_{max}^2} = \ln \frac{AR}{E} + \ln\left[n(1-\alpha_{max})^{n-1}\right] - \frac{E}{RT_{max}} \quad (7)$$

where T_{max} is the temperature at the inflection point of the thermodegradation curves, which corresponds to the maximum reaction rate. From a plot of $\ln(\beta/T_{max}^2)$ versus $1/T_{max}$ and fitting the data to a straight line, the activation energy can be calculated from the slope. Now, it is well known that this model can be also used when $f(\alpha)$ correspond to other kinetic models.[41]

Flynn–Wall–Ozawa equation:

$$\ln \beta = \ln \frac{0.0048AE}{g(\alpha)R} - 1.0516\frac{E}{RT} \quad (8)$$

This is one of the integral methods by which the activation energy can be determined without knowing the reaction order. The activation energy can be calculated for different conversions from the plot of $\ln \beta$ versus $1/T$.

Another method used to evaluate the kinetic parameters is the IKP (invariant kinetic parameters) method.[42,43] According to this procedure, the values of the activation parameters, obtained from various forms of $f(\alpha)$, are correlated through an apparent compensation effect:

$$\ln A = \alpha^* + \beta^* E \quad (9)$$

where α^* and β^* are constants (the compensation effect parameters).

To apply this method, at each heating rate (β_i), we plotted the values of $\ln A_i$ versus E_i. These parameters were obtained using the Coats–Redfern methodology for different kinetic models studied (Table I). From the intersect at the origin and the slope, the α_i^* and β_i^* val-

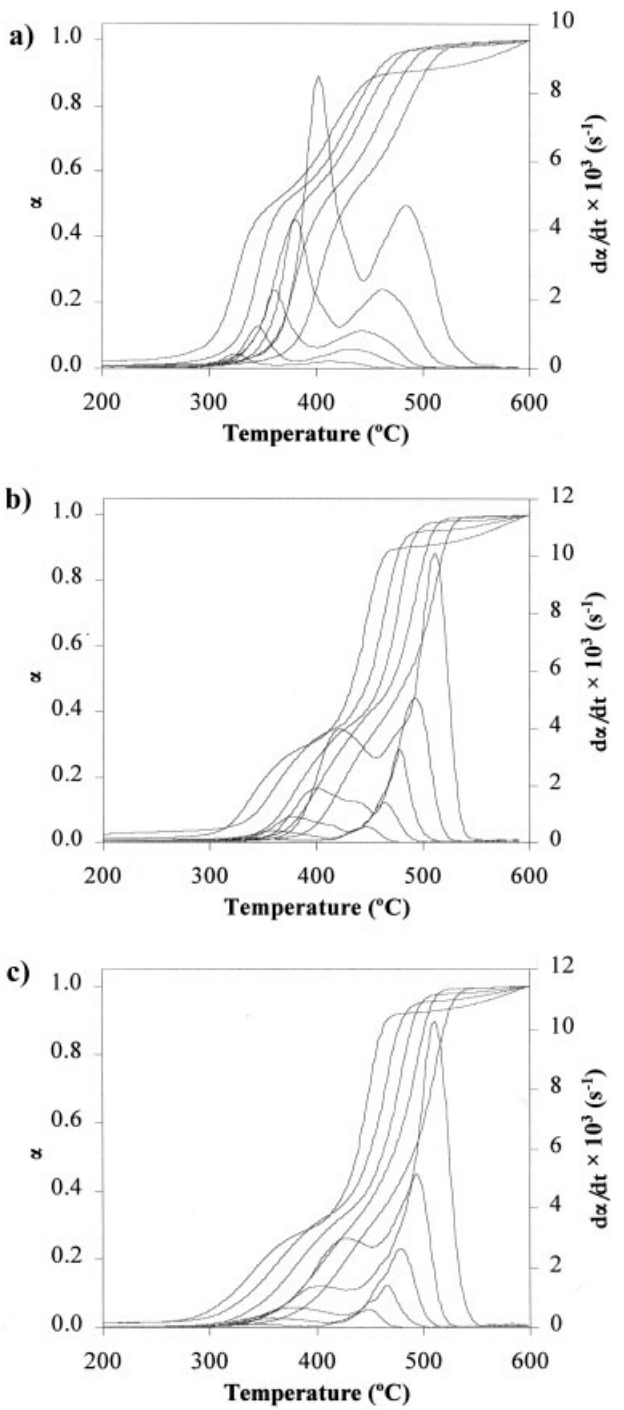

Figure 2 Degree of conversion (α) versus temperature and derivative curve for the decomposition of PEA(glc-*n*) samples conducted under N_2 at different heating rates. Curves are drawn from left to right in increasing order of heating rates: (a) PEA(glc-6), (b) PEA(glc-11), and (c) PEA(glc-12).

TABLE II
Thermogravimetric Data of PEA(glc-*n*) Samples

Polymer	β (°C/min)	T_{onset} (°C)	$T_{20\%}$ (°C)	$T_{50\%}$ (°C)	$T_{70\%}$ (°C)	T_{max}[a] (°C)
PEA(glc-6)	2	207	319	359	411	326/412
	5	220	339	370	423	345/434
	10	232	356	388	433	357/442
	20	240	375	408	451	382/460
	40	260	397	429	471	404/485
PEA(glc-11)	2	214	352	435	448	339/443
	5	225	367	450	464	360/466
	10	239	388	462	476	376/476
	20	264	406	472	490	400/494
	40	278	428	485	506	424/511
PEA(glc-12)	2	224	351	438	450	337/450
	5	246	366	449	465	362/463
	10	252	385	461	477	378/480
	20	277	408	471	490	405/494
	40	289	428	490	508	427/511

[a] Temperatures corresponding to the first and second steps, respectively.

ues were determined. Furthermore, the straight lines $\ln A_i$ versus E_i for each heating rate should intersect in a point which corresponds to the true values of A and E. These are called the invariant activation parameters (A_{inv}, E_{inv}). Certain variations of the experimental conditions actually determine a region of intersection in the ln A, E space. For this reason, the evaluation of the invariant activation parameters is performed using the following relation:

$$\ln A_{inv} = \alpha_i^* + \beta_i^* E_{inv} \quad (10)$$

Thus, a plot α_i^* versus β_i^* is actually a straight line whose parameters allow evaluation of the invariant activation parameters.

RESULTS AND DISCUSSION

Thermal degradation studies

Thermogravimetric scans (Fig. 1) indicated that, between room temperature and 600°C, the three studied polymers undergo two major weight-loss processes in a nitrogen atmosphere; all the polymers presenting the same basic shape for the TGA curve. Experiments performed in air showed also the same characteristics, only a slightly higher amount of residue could be found.

The analysis of the degradation process is rather complicated since two different stages could be observed. These overlapping processes do not permit the use of isothermal procedures and consequently only nonisothermal analysis was performed. Figure 1 indicates that when the heating rate decreases, the temperature at which the degradation occurs also decreases. The first process is more important in the polymer whose repeat unit has the highest weight percentage in glycolic acid residues (the PEA(glc-*n*) sample with the lowest *n* value), and consequently this step seems to be associated with their decomposition. Thus, the three studied poly(ester amide)s were stable up to approximately 200–300°C and had lost about 45% of their weight by the end of the first stage in the case of PEA(glc-6) and about 30% for the PEA(glc-11) and PEA(glc-12). At the end of the degradation process almost 0–14% residue remained for PEA(glc-6) and PEA(glc-11), whereas a 5–8% residue remained for PEA(glc-12).

Figure 2 plots the degree of conversion versus temperature (TG curve) together with the corresponding derivative of this curve (DTG curve) for the three polymers at all the assayed heating rates. In the DTG curve, each stage of the process showed a clear peak at a temperature that increased with the heating rate. The height of the peaks indicated that the degradation pro-

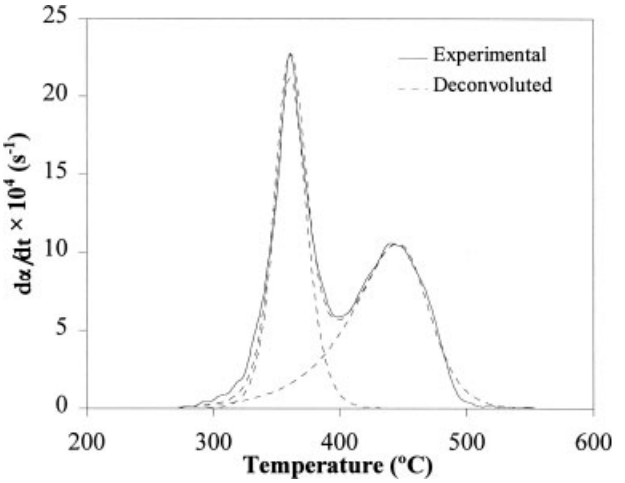

Figure 3 Deconvolution of the DTA curve corresponding to the thermal decomposition of PEA(glc-6) at 10°C/min.

cess in the first stage was faster for the PEA(glc-6) sample. In contrast, the second stage was the faster for the PEA(glc-11) and PEA(glc-12) poly(ester amide)s.

The characteristic TG temperatures of the three polymers are summarized in Table II. The degradation started at around 200°C, the onset temperature increasing with the heating rate and the number of methylenes of the repeat unit of the polymer. The two maxima of the derivative curves occurred at similar temperatures for the aminoundecanoic acid and the aminododecanoic acid derivatives, whereas the corresponding values were slightly lower for the aminohexanoic acid derivative.

To solve the overlapping problem, a mathematical deconvolution of the DTG curves was carried out. Figure 3 shows the separation of peaks of the curve at 10°C/min for PEA(glc-6), by way of example. The sum of the separated curves reproduces the experimental signal quite well. Similar results were obtained for the three poly(ester amide)s studied at different heating rates.

The Kissinger method was the first to be employed to analyze the TG data because it is independent of any thermodegradation mechanism. Equation (7) was used as explained before. Plots of $\ln(\beta/T_{max}^2)$ versus $1000/T_{max}$ are shown in Figure 4(a). This method gives the

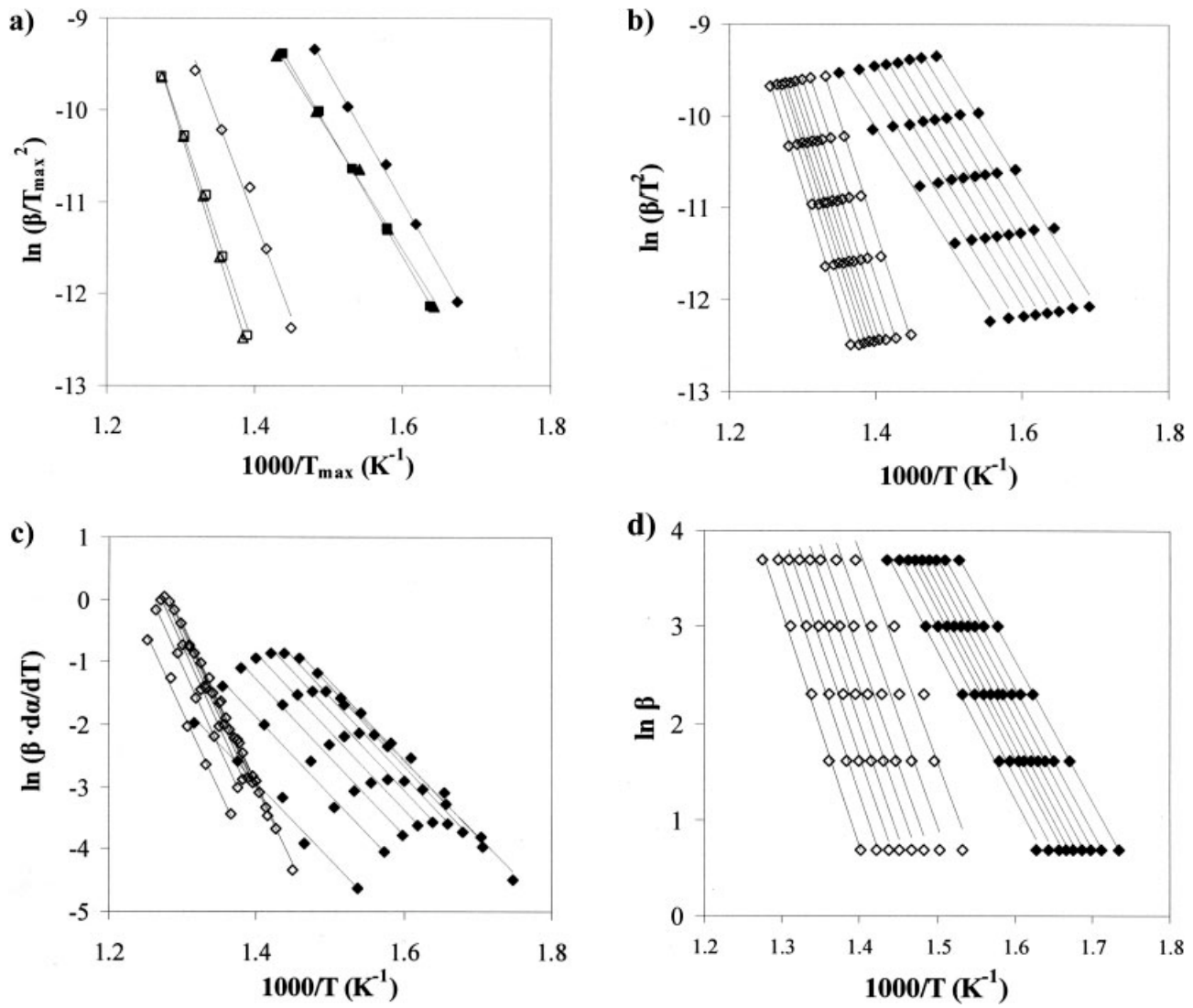

Figure 4 (a) Plots of $\ln(\beta/T_{max}^2)$ versus $1000/T_{max}$ (Kissinger method) for the first (full symbols) and the second (empty symbols) decomposition step of PEA(glc-6) (◆), PEA(glc-11) (■) and PEA(glc-12) (▲). (b) Plots of $\ln(\beta/T^2)$ versus $1000/T$ (KAS method) for the first (◆) and the second (◇) thermal decomposition steps of PEA(glc-11). Conversions ranged from 0.1 to 0.9, although conversion of 0.9 is not drawn in the first step for the sake of clarity. (c) Plots of $\ln(\beta\, d\alpha/dT)$ versus $1000/T$ (Friedman method) for the first (◆) and the second (◇) thermal decomposition steps of PEA(glc-12). Conversions ranged from 0.1 to 0.9. (d) Plots of logarithms of the heating rates, ln β, versus $1000/T$ (Ozawa plot) for the first (◆) and the second (◇) thermal decomposition steps of PEA(glc-6). Conversions ranged from 0.1 to 0.9, although conversion of 0.1 is not drawn in the second step for the sake of clarity.

TABLE III
Activation Energies of the Studied Polymers Determined by Isoconversional Methods

Polymer	Step[a]	E (kJ/mol) Kissinger[b]	KAS[c]	Ozawa[c]	Friedman[c]
PEA (glc-6)	1	118	116	120	120
	2	176	179	181	185
PEA (glc-11)	1	114	107	112	107
	2	204	207	208	214
PEA (glc-12)	1	106	100	106	103
	2	216	210	212	213

[a] The two steps of degradation are referred to as 1 and 2 in increasing order of temperature.
[b] Calculated at the temperature corresponding to the maximum of each step in the DTG curve.
[c] E values summarized correspond to mean values obtained from different degrees of conversion.

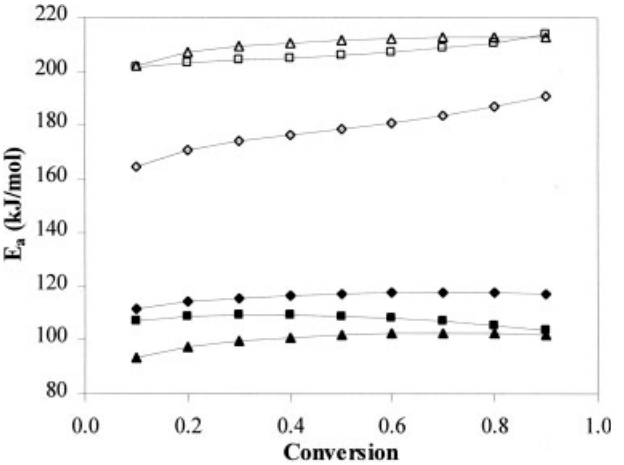

Figure 5 Plots of the activation energy, calculated with the KAS methodology, versus conversion for the first (full symbols) and the second (empty symbols) decomposition steps of PEA(glc-6) (◆), PEA(glc-11) (■), and PEA(glc-12) (▲).

associated activation energy only at the maximum of the DTG curve for each step.

To calculate the activation energy during the whole process at different conversion degrees, the KAS method [eq. (5)] was also applied by plotting $\ln(\beta/T^2)$ versus $1000/T$. Figure 4(b) shows the corresponding straight lines obtained for PEA(glc-11) as an illustrative example.

It is also possible to obtain this information by applying the Friedman method [eq. (6)], which enables the values of activation energies to be determined from plots of $\ln(\beta\, d\alpha/dT)$ versus $1000/T$ over a wide range of conversions. Straight lines are obtained at each degree of conversion for the two degradation steps, as shown in Figure 4(c) for PEA(glc-12).

A method also independent of the degradation mechanism is that proposed by Flynn–Wall–Ozawa [eq. (8)], where the activation energy can be obtained from the plot of ln β versus $1000/T$. Linear relationships were obtained for each degradation stage at a constant degree of conversion. Figure 4(d) illustrates the results obtained for PEA(glc-6).

The activation energy values calculated by the above methods for the three studied poly(ester amide)s are summarized in Table III. As can be seen, the values determined by different equations are similar. The relationship of E and conversion (KAS method) is shown in Figure 5. The results obtained indicate that the activation energy of thermal degradation for the first stage is always lower than that corresponding to the second stage. Furthermore, the activation energy in the first step slightly decreases as the number of methylenes of the repeat unit of the polymer increases. The

TABLE IV
Activation Energies of PEA(glc-11) in N_2 Atmosphere Obtained by Coats–Redfern Method (First Step)

	2°C/min		5°C/min		10°C/min		20°C/min		40°C/min	
	E (kJ/mol)	r	E (kJ/mol)	r	E (kJ/mol)	r	E (kJ/mol)	r	E (kJ/mol)	r
Power	38	0.9102	38	0.9230	42	0.9264	44	0.9401	35	0.8868
$A_{3/2}$	84	0.9724	84	0.9796	91	0.9802	88	0.9791	80	0.9651
A_2	60	0.9699	61	0.9777	65	0.9784	63	0.9772	57	0.9614
A_3	37	0.9640	37	0.9789	40	0.9742	39	0.9724	34	0.9521
A_4	25	0.9563	25	0.9669	27	0.9686	26	0.9661	23	0.9392
F_1	131	0.9745	132	0.9813	142	0.9818	138	0.9809	126	0.9683
R_2	107	0.9547	107	0.9637	116	0.9648	117	0.9686	102	0.9449
R_3	115	0.9620	115	0.9800	124	0.9711	124	0.9731	110	0.9536
D_1	185	0.9359	184	0.9463	199	0.9477	209	0.9574	176	0.9246
D_2	219	0.9546	219	0.9645	236	0.9640	243	0.9794	210	0.9473
D_3	240	0.9652	240	0.9729	259	0.9736	259	0.9754	231	0.9582
D_4	219	0.9558	219	0.9645	236	0.9653	241	0.9698	210	0.9473
$n = 1.5$	160	0.9878	162	0.9923	173	0.9925	163	0.9895	156	0.9841
$n = 1.5$, $m = 0.5$	92	0.9948	93	0.9976	99	0.9977	89	0.9943	89	0.9923
$n = 1.9$; $m = 0.1$	174	0.9953	176	0.9979	187	0.9980	170	0.9950	170	0.9932
$n = 2$	194	0.9954	196	0.9979	209	0.9980	190	0.9950	190	0.9933
$n = 3$	272	0.9999	277	0.9996	294	0.9996	252	0.9996	270	0.9995

TABLE V
Activation Energies (kJ/mol) of the Studied Polymers Determined by the Coats–Redfern Method at 2°C/min.

	PEA (glc-6)				PEA (glc-11)				PEA (glc-12)			
	Step 1		Step 2		Step 1		Step 2		Step 1		Step 2	
Model	E	r	E	r	E	r	E	r	E	r	E	r
Power	75	0.9723	42	0.9929	38	0.9102	102	0.9895	39	0.9778	102	0.9947
$A_{3/2}$	152	0.9964	85	0.9992	84	0.9724	200	0.9998	77	0.9965	196	0.9992
A_2	111	0.9963	61	0.9991	60	0.9699	147	0.9998	55	0.9961	144	0.9991
A_3	71	0.9959	37	0.9990	37	0.9640	94	0.9998	34	0.9959	92	0.9991
A_4	51	0.9954	25	0.9989	25	0.9563	67	0.9998	23	0.9939	66	0.9990
F_1	232	0.9966	134	0.9992	131	0.9745	306	0.9998	121	0.9968	300	0.9992
R_2	193	0.9884	113	0.9992	107	0.9547	257	0.9975	106	0.9913	254	0.9994
R_3	205	0.9917	119	0.9997	115	0.9620	272	0.9988	109	0.9935	268	0.9998
D_1	331	0.9770	201	0.9953	185	0.9359	444	0.9912	188	0.9846	443	0.9956
D_2	380	0.9855	234	0.9984	219	0.9546	505	0.9957	216	0.9906	501	0.9984
D_3	421	0.9921	250	0.9997	240	0.9652	556	0.9988	228	0.9941	548	0.9998
D_4	387	0.9876	232	0.9990	219	0.9558	514	0.9969	228	0.9841	509	0.9991
$n = 1.5$	279	0.9998	159	0.9951	160	0.9878	363	0.9978	140	0.9995	354	0.9949
$n = 1.5$; $m = 0.5$	162	0.9990	88	0.9867	92	0.9948	209	0.9920	76	0.9999	202	0.9969
$n = 1.9$; $m = 0.1$	299	0.9991	167	0.9879	174	0.9953	386	0.9923	145	0.9990	373	0.9875
$n = 2$	333	0.9991	187	0.9880	194	0.9954	430	0.9924	162	0.9999	416	0.9876
$n = 3$	459	0.9917	252	0.9712	272	0.9999	584	0.9778	211	0.9965	558	0.9701

second degradation step always has a significantly higher activation energy than the first one. PEA(glc-11) and PEA(glc-12) showed similar values, whereas a lower value was found for PEA(glc-6), which has a clearly lower methylene content.

The Coats–Redfern method was chosen to determine the thermal degradation mechanism involved in the different stages for the three studied polymers. According to eq. (4), the activation energy for every $g(\alpha)$ function listed in Table I can be calculated at constant heating rates by fitting a linear plot of $\ln g(\alpha)/T^2$ versus $1/T$. The slope of this representation allows the activation energy to be determined for each possible model and the model to be selected by considering the agreement with the previously calculated activation energy (Table III). Furthermore, good regression coefficients are required. Note that this methodology enables the complete kinetic triplet (E, A, and $g(\alpha)$) to be known if the intercept at the origin of the linear plot is also considered.

To find the influence of the heating rate, we applied the Coats–Redfern methodology to the five heating rates considered (for conversions between 0.1 and 0.9). Table IV shows the corresponding data for the first decomposition stage of PEA(glc-11) as an illustrative example. It can be seen that at all heating rates similar E values were found, a feature that was also observed for the second step and for the other two

TABLE VI
Kinetic Parameters Associated with the Thermal Degradation of the Three Studied Polymers

	E_{inv} (kJ/mol)	$\ln A_{inv}$ (min^{-1})	k (min^{-1})	Model	E (kJ/mol)	$\ln A$ (min^{-1})
Step 1[a]						
PEA(glc-6)	118	21.03		A_2	111	19.64
PEA(glc-11)	110	17.91	10.020	R_2	107	16.71
				R_3	115	17.92
PEA(glc-12)	98	15.95	0.029	R_2	104	16.44
				R_3	109	17.22
Step 2[b]						
PEA(glc-6)	169	26.52	0.11	$n = 1.9$; $m = 0.1$	167	27.31
PEA(glc-11)	213	32.96	0.039	$A_{3/2}$	200	30.99
				$n = 1.5$; $m = 0.5$	209	33.63
PEA(glc-12)	214	33.11	0.038	$A_{3/2}$	196	30.27
				$n = 1.5$; $m = 0.5$	202	32.32

[a] Rate constant calculated at $T = 334$°C and using the Arrhenius equation ($k = A_{inv} \exp(-E_{inv}/RT)$).
[b] Rate constant calculated at $T = 435$°C and using the Arrhenius equation ($k = A_{inv} \exp(-E_{inv}/RT)$).

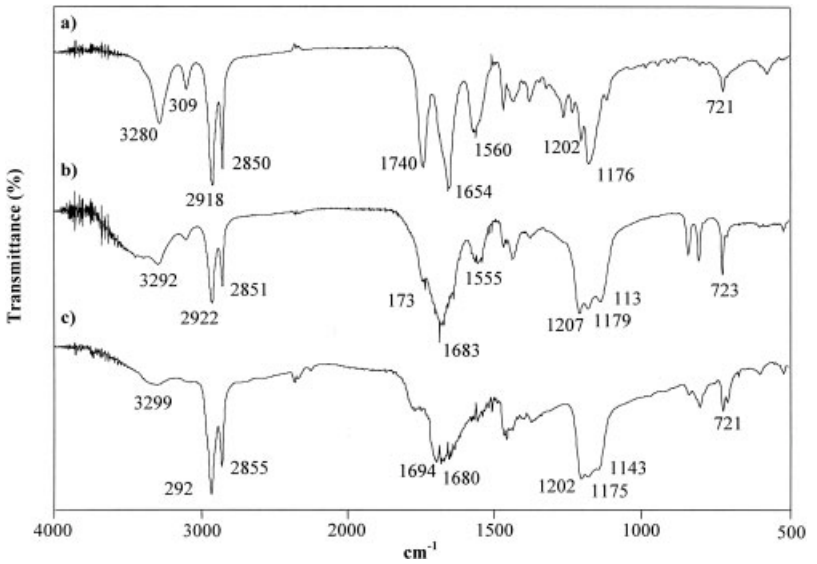

Figure 6 Infrared spectra of PEA(glc-12) films before (a) and after different degrees of thermal decomposition, which correspond to weight losses of 10% (b) and 30% (c).

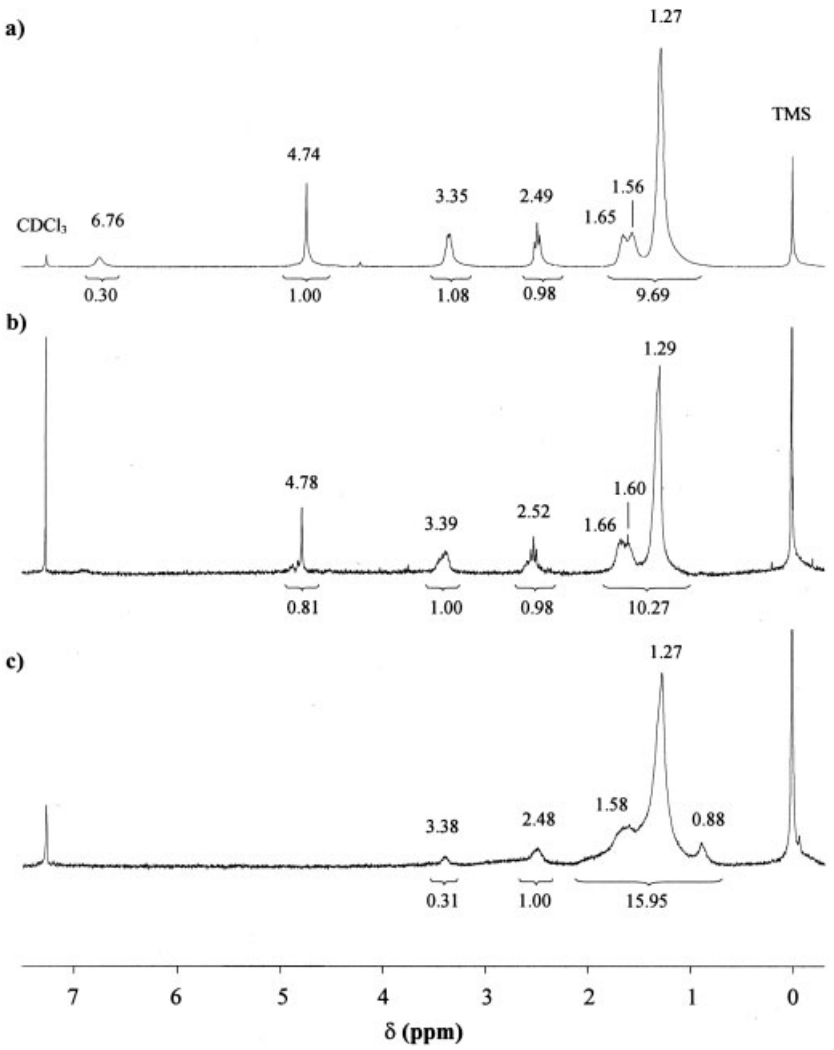

Figure 7 ^{1}H NMR spectra of PEA(glc-12) samples before (a) and after different degrees of thermal decomposition, which correspond to weight losses of 10% (b) and 30% (c). TFA/$CDCl_3$ was used as a solvent.

studied polymers. However, the activation energies obtained at 2°C/min were in slightly better agreement with the values previously obtained (Kissinger, KAS, Friedman, and Flynn–Wall–Ozawa methods). For comparison purposes, we only considered the data at this heating rate (Table V). Works performed with poly(dodecamethylene–isophthalamide)[44] and poly(*p*-dioxanone)[32] indicated that the best agreement was also achieved at the low heating rates.

The kinetic parameters that fit better with experimental non isothermal data are summarized in Table VI for each step and polymer. It can be seen that in some cases two models appear suitable since their E values are close to the isoconversional ones. To discriminate the kinetic model the IKP method was used, the invariant parameters also being summarized in Table VI. This method let us to choose the most appropriate model for each step and polymer.

The kinetic parameters showed differences between the two steps, namely the first step had lower E and A values than the second one had. To compare the thermal stability of the two processes for the same polymer and between different polymers, the value of the activation energy should not be used exclusively due to the compensating effect that exists between E and A. Thus, values of kinetic constants are also indicated for comparison purposes. These constants were calculated using the Arrhenius equation at temperatures which correspond to the average of the T_{max} determined for the three polymers at each step (i.e., 334 and 435°C). Note that the kinetic model ($f(\alpha)$) is not considered in the equation, and consequently precautions should be taken when reactions with a different mechanism are compared.

The analysis of the results obtained by the Coats–Redfern and IKP methodologies showed that the degradation mechanisms of PEA(glc-11) and PEA(glc-12) are the same. In the first degradation step, both poly (ester amide)s follow a deceleration (R_2) type mechanism, whereas an autocatalytic ($n = 1.5$; $m = 0.5$) mechanism can be chosen for the second step. PEA(glc-6) had a different behavior, which may be associated to its higher weight percentage in glycolic acid units and the lower methylene content of its amino acid residues. Thus, the first step follows a sigmoidal type (A_2) mechanism that contrasts with the surface control (R_2) thermal degradation mechanism found for the other two polymers. This mechanism is decelerative and presents the maximum rate at the start, which is not the case of the A_2 mechanism. The second step fits to an autocatalytic ($n = 1.9$; $m = 0.1$) mechanism that is similar to that found for the other two polymers.

The first stage of degradation had similar activation energies for the three polymers, but the preexponential factor was clearly higher for PEA(glc-6). The kinetic rate constant calculated at 334°C was 0.094 min^{-1}, a value considerably higher than those determined for the aminoundecanoic and the aminododecanoic acid derivatives (0.020 and 0.029 min^{-1}, respectively). In this case, from the great difference found between the kinetic constants, it can be inferred that PEA(glc-6) has the fastest degradation rate for the first step in spite of the inaccuracy caused by the different reaction mechanism. Furthermore, when $f(\alpha)$ is considered at conversions between 0.1 and 0.9, the degradation rate varies in the 0.05–0.03 and 0.03–0.01 min^{-1} ranges for the aminohexanoic acid and aminododecanoic acid derivatives, respectively. For the second step, PEA(glc-6) had the lowest activation energy and also the lowest frequency factor. The calculated rate constant was slightly higher than those determined for the PEA(glc-11) and PEA(glc-12) samples. PEA(glc-11) and PEA(glc-12) poly(ester amide)s with the same reaction mechanisms at each step showed similar thermal stability.

Infrared (Fig. 6) and ^1H NMR (Fig. 7) spectra were taken at different stages of thermal degradation to know how it proceeds. The observed weight losses in the thermograms of Figure 1 strongly suggest that the second degradation step mainly corresponds to the decomposition of the polymethylenic segments since the associated weight loss is higher for the polymer

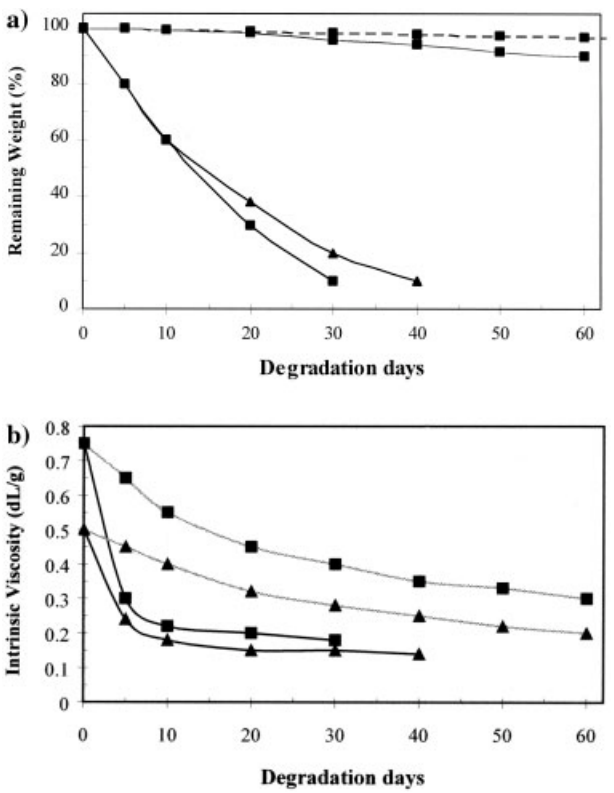

Figure 8 Remaining weight percentage (a) and intrinsic viscosity (b) of PEA(glc-6) (■) and PEA(glc-11) (▲) samples versus days of exposure in phosphate buffer (pH 7.4) at 37°C (– – –), sodium citrate buffer (pH 2.3) at 37°C (· · · · · ·), and distilled water at 70°C (——). Plotted data correspond to single run experiments.

constituted by longer ω-amino acid units. Infrared spectra clearly show that absorption bands associated to amide groups (i.e., the amide A and amide II bands at 3280 and 1560 cm^{-1}) disappear at the end of the first degradation step. Furthermore, the C=O absorption band of ester (1740 cm^{-1}) and the amide I (1654 cm^{-1}) groups change to an intermediate position. It should be pointed out that methylene bands (2918, 2850, and 721 cm^{-1}) are still well defined after this stage of degradation and that C—O bands (1200–1140 cm^{-1}) remain.

Proton spectra also show the disappearance of the NH groups (6.76 ppm), in agreement with the infrared observations. In addition, the signal of glycolyl protons (4.74 ppm) decreases during degradation and also disappears at the end of the first degradation step. Obviously, the signal of the $NHCH_2$ protons also decreases at this stage whereas the relative area of protons associated to the polymethylenic segments increases.

Hydrolytic and enzimatic degradation studies

Figure 8 shows the remaining weight percentages of the PEA(glc-6) samples after immersion in different aqueous media. A significant weight loss was observed only under the accelerated degradation conditions at a high temperature (70°C) because of the greater ability of the medium to dissolve the degradation products. The samples were completely dissolved after 40 days of exposure. Nevertheless, the weight loss was also not high under the accelerated conditions in acidic medium (pH of 2.3) if the temperature was maintained at 37°C. Thus, after 60 days of exposure, only a 10% weight loss was detected. Weight changes in the pH 7.4 buffered medium at 37°C were logically not appreciable for exposure periods less than one month. Intrinsic viscosity changes (Fig. 8) demonstrated that the polymer degrades under both accelerated conditions, the change being faster in the high temperature me-

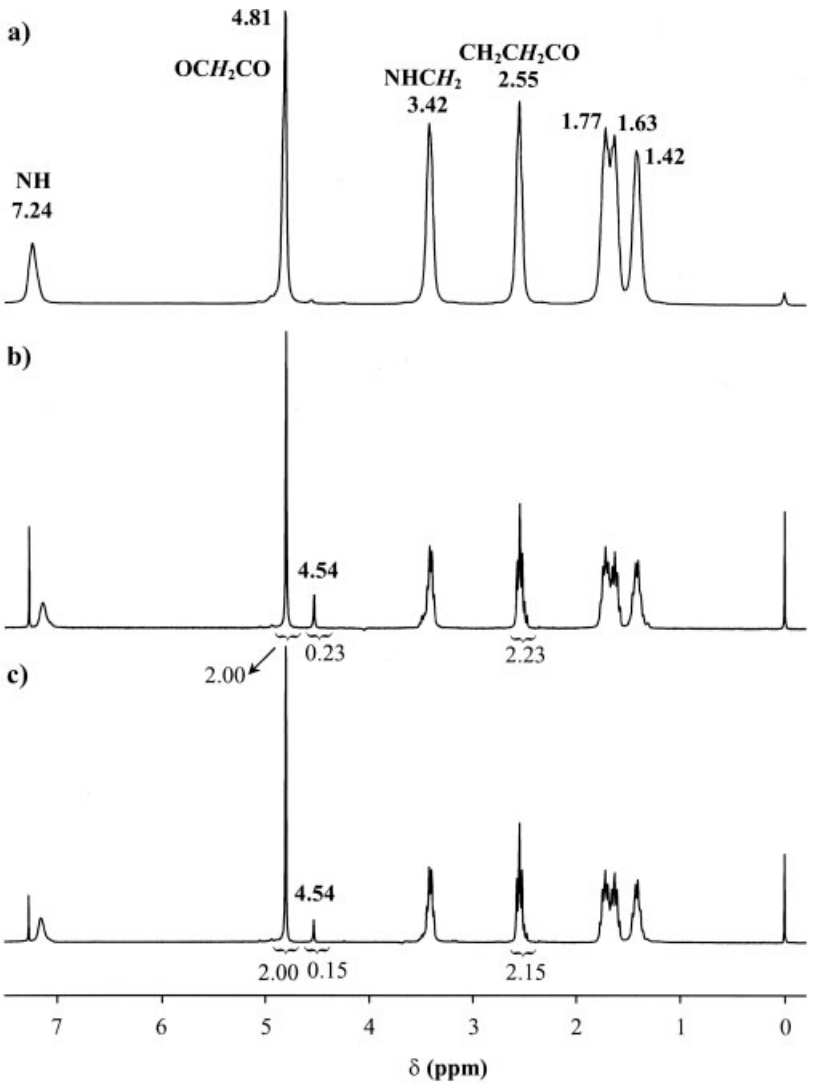

Figure 9 ^1H NMR spectra of a PEA(glc-6) sample before (a) and after exposure for 13 days in distilled water at 70°C (b) and 60 days in sodium citrate buffer (pH 2.3) at 37°C (c). TFA/$CDCl_3$ was used as a solvent.

dium. It is worth mentioning that the intrinsic viscosity tends to a constant value, which may correspond to the minimum size at which the degraded polymer chain is still insoluble. This limit is higher at 37°C (0.3 dL/g) than at 70°C (0.18 dL/g).

Figure 8 also shows that PEA(glc-11) degrades quite similarly to the aminohexanoic derivative. However, the weight loss is slightly smaller probably due to the decrease in the solubility of the less polar fragments produced. Thus, a remaining weight of 10% was found after 40 days of exposure to distilled water at 70°C. Note also that the intrinsic viscosities fall to lower values than those observed for the aminohexanoic derivatives (Fig. 11b). In this case, the shorter segments should still be insoluble, which justifies the lower viscosity limit.

^{1}H NMR spectra of the PEA(glc-*n*) polymers show the appearance of a new signal at 4.54 ppm during the hydrolytic degradation process. This peak can be attributed to a $COCH_2OH$ terminal group and consequently points to an ester bond cleavage. Figure 9 shows the spectra of the original and some degraded samples, as example. It can also be seen that the signals attributed to the methylene protons of the aminohexanoic acid units have better resolution after degradation. It is possible to distinguish triplets for the CH_2CH_2CO protons, a feature in agreement with the low molecular weight of these samples. The ratio between glycolic acid and the ω-amino acid units (measured through the area of OCH_2CO and CH_2CH_2COO protons) remains practically constant throughout the degradation process. This feature suggests that highly soluble $HOCH_2COOH$ units are not generated during degradation, and consequently amide and ester bond cleavages cannot be produced at the same time.

Number average molecular weights of the degraded PEA(glc-6) samples can be estimated from the area of the signals corresponding to terminal ($A_{4.54}$) and nonterminal ($A_{4.81}$) glycolyl protons by the equation:

$$M_n = 189 + [171 \times (A_{4.81}/A_{4.54})] \qquad (11)$$

which can be derived by assuming that all terminal groups correspond to ester bond cleavages and considering a molecular weight of 171 g/mol for the repeat unit. In this way, values of 2470 and 1675 g/mol can be estimated for the degraded samples in a pH 2.3 medium at 37°C and distilled water at 70°C, respectively, which have asymptotic intrinsic viscosity values of 0.30 and 0.18 g/dL.

Scanning electron micrographs of polymers exposed to the pH 2.3 medium [e.g., PEA(glc-6) in Fig. 10(a)]

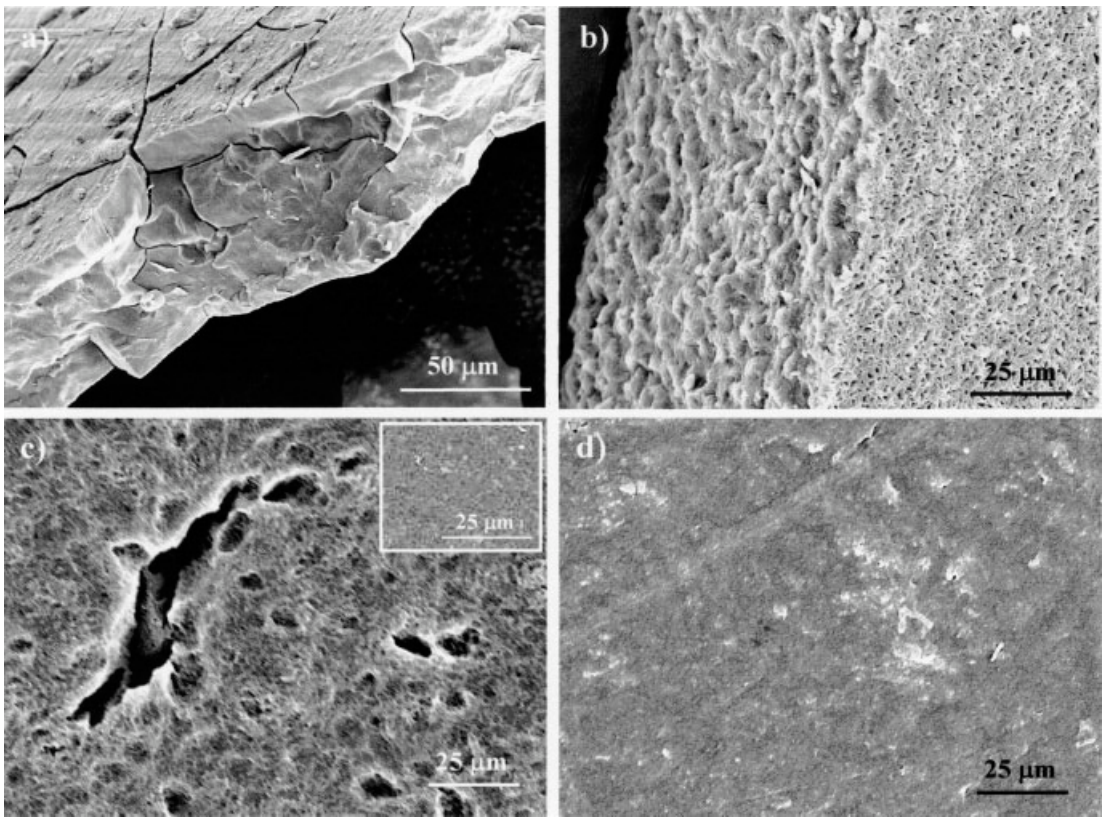

Figure 10 Scanning electron micrographs of PEA(glc-6) (a, c) and PEA(glc-11) (b, d) disks exposed to a sodium citrate buffer at 37°C for 60 days (a), distilled water at 70°C for 10 days (b) and a proteinase K medium for 16 days (c, d). Inset in (c) corresponds to a PEA(glc-6) sample before exposure to the degradation medium.

showed that the disk samples remain practically unaltered, as expected from the detected low weight loss. It is also clear that samples become highly brittle, probably as a consequence of the molecular weight decrease. On the contrary, the samples exposed to distilled water at 70°C showed that they were highly porous inside [e.g., PEA(glc-11) in Fig. 10(b)], which justified the weight losses detected during degradation. The ester bond cleavages produce acid groups that may enhance degradation in the inner part of the disk due to the lower pH caused by a local concentration of acid groups. Note that the level of erosion seems higher in the inner part than on the surface where holes mainly appear as a consequence of the degradation that occurs inside. It is well known[45] that polyesters derived from glycolic or lactic acid usually show an autocatalytic effect.

Degradation was also evaluated in enzymatic media with a protease and an esterease activity. Only weight losses were evaluated since enzymatic degradation takes place on the disk surfaces. Results indicate that both polymers were susceptible to the attack of both kinds of enzymes, although degradation is enhanced in the proteinase K medium, an enzyme capable of hydrolyzing both amide and ester bonds.[22]

The weight percentage of the PEA(glc-6) sample with an intrinsic viscosity of 0.75 dL/g decreased to 95 and 80% after 21 days of exposure in a *P. cepacia* medium and a proteinase K medium (Fig. 11), respectively. The PEA(glc-11) samples, which have a lower molecular weight, degraded at a slower rate, the corresponding remaining weights being 98 and 92% after the same exposure time. Scanning electron micrographs of the disk surfaces [Figs. 10(c) and (d)] confirm the different erosion of the PEA(glc-6) and PEA(glc-11) samples. Thus, Figure 10(c) shows numerous holes of different sizes on the surface of a PEA(glc-6) disk after exposure for 16 days in a proteinase K medium (14 wt % loss), whereas the surface of a PEA(glc-11) disk [Fig. 10(d)] remained practically unaltered (6 wt % loss) after the same exposure time.

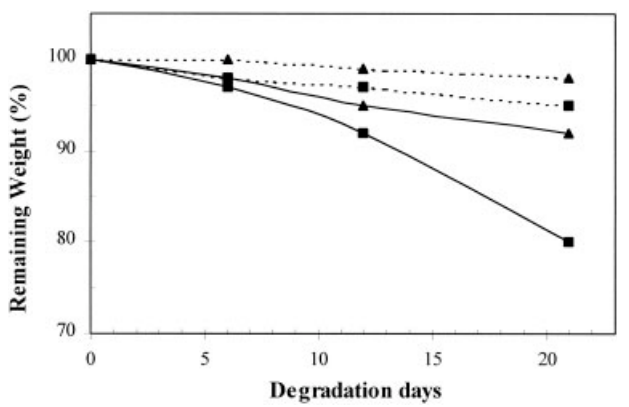

Figure 11 Remaining weight percentage of PEA (glc-6) (■) and PEA (glc-11) (▲) samples versus days of exposure in a lipase from *P. cepacia* (– – –) and a proteinase K (——) media. Plotted data correspond to single run experiments.

CONCLUSIONS

The thermal degradation kinetic parameters of the three studied poly(ester amide)s, obtained with different methodologies, are highly consistent. In all cases, the polymers show two degradation stages, the second one of which involves the decomposition of the polymethylenic segment, and consequently becomes more important for samples with longer ω-amino acid residues.

The kinetic parameters indicate differences between the two stages of the degradation process. The first stage presents lower values of E and ln A than did the second one.

Analysis of experimental results suggests that PEA(glc-6) follows a kinetic model of sigmoidal type, A_2, in the first stage of degradation, and an autocatalytic kinetic model ($n = 1.9$; $m = 0.1$) in the second stage. In contrast, in the case of PEA(glc-11) and PEA(glc-12), the degradation process follows a deceleration function, R_2, and an autocatalytic kinetic model ($n = 1.5$; $m = 0.5$), for the first and the second steps, respectively. The results also indicate a similar thermal stability of PEA(glc-11) and PEA(glc-12).

The new poly(ester amide)s are hydrolytically degradable through the cleavage of ester bonds. The degradation process is accelerated by high temperatures, which also enhance the solubility of the small fragments generated during hydrolysis. An autocatalysis effect seems to take place in the hydrolytic degradation at 70°C. Furthermore, the polymers are susceptible to the enzymatic attack of proteases like proteinase K and become more resistant to lipases like *P. cepacia*, which have only an estearase activity.

References

1. Huang, S. J. Encyclopedia of Polymer Science and Engineering, Vol. 2; Wiley-Interscience: New York, 1985.
2. Chu, C. C. Wound Closure Materials and Devices; CRC Press: Boca Raton, FL, 1997; pp 65–106.
3. Schmitt, E. E.; Polistina, R. A.U.S. Pat. 3,297,033 (1967).
4. Ray, J. A.; Doddi, N.; Regula, D.; Williams, J. A.; Melverger, A. Surg Gynecol Obstet 1981, 153, 497.
5. Schneider, A. K.U.S. Pat. 2,703,316 (1955).
6. Bezwada, R. S.; Jamiolkowski, D. D.; Lee, I. Y.; Agarwal, V.; Persivale, J.; Trenka-Bethin, S.; Erneta, M.; Persivale, J.; Suryadevara, J.; Yang, A.; Liu, S. Biomaterials 1995, 16, 1141.
7. Rosensaft, P. L.; Webb, R. L.U.S. Pat. 4,243,775 (1981).
8. Grigat, E.; Koch, R.; Timermann, R. Polym Degrad Stab 1998, 59, 223.
9. Kakimoto, M. A.; Nagi, Y. S.; Imai, Y. J Polym Sci Part A: Polym Chem 1986, 34, 1511.
10. Gonsalves, K. E.; Chen, X.; Cameron, J. A. Macromolecules 1992, 25, 3309.
11. Bera, S.; Jedlinski, Z. J Polym Sci Part A: Polym Chem 1993, 31, 731.

12. Katsarava, R.; Beridze, V.; Arabuli, N.; Kharadze, D.; Chu, C. C.; Won, C. Y. J Polym Sci Part A: Polym Chem 1999, 37, 391.
13. Stapert, H. R.; Dijkstra, P. J.; Feijen, J Macromol Symp 2000, 152, 127.
14. Gomurashvili, Z.; Katsarava, R. J Macromol Sci Pure Appl Chem 2000, 37, 215.
15. Lee, S. Y.; Park, J. W.; Yoo, Y. T.; Im, S. S. Polym Degrad Stab 2002, 78, 63.
16. Lips, P. A. M.; Broos, R.; van Heeringen, M. J. M.; Dijkstra, P. J.; Feijen, J. Polymer 2005, 46, 7823.
17. Villuendas, I.; Molina, I.; Regaño, C.; Bueno, M.; Martínez de Ilarduya, A.; Galbis, J.; Muñoz-Guerra, S. Macromolecules 1999, 32, 8033.
18. Villuendas, I.; Bou, J.; Rodríguez-Galán, A.; Muñoz-Guerra, S. Macromol Chem Phys 2001, 202, 236.
19. Vera, M.; Almontassir, A.; Rodríguez-Galán, A.; Puiggalí, J, Macromolecules 2003, 36, 9784.
20. Paredes, N.; Rodríguez-Galán, A.; Puiggalí, J, J Polym Sci Part A: Polym Chem 1998, 37, 2521.
21. Paredes, N.; Rodríguez-Galán, A.; Puiggalí, J.; Peraire, C. J Appl Polym Sci 1999, 74, 2312.
22. Asín, L.; Armelin, E.; Montané, J.; Rodríguez-Galán, A.; Puiggalí, J. J Polym Sci Part A: Polym Chem 2001, 39, 4283.
23. Barrows, T. H.U.S. Pat. 4,529,792 (1985).
24. Barrows, T. H.; Truong, M.Int. Pat. WO 93/13814 (1993).
25. Roby, M. S.; Jiang, Y.U.S. Pat. 5,902,874 (1999).
26. Roby, M. S.; Jiang, Y.U.S. Pat. 5,914,387 (1999).
27. Int-Velt, J. P. A.; Shen, Z. R.; Takens, G. A. J.; Dijkstra, P.; Feijen, J. J Polym Sci Part A: Polym Chem 1994, 32, 1063.
28. Dijkstra, P. J.; Feijen, J. Macromol Symp 2000, 155, 67.
29. Vera, M.; Rodríguez-Galán, A.; Puiggalí, J. Macromol Rapid Commun 2004, 25, 812.
30. Ramis, X.; Salla, J. M.; Puiggalí, J. J Polym Sci Part A: Polym Chem 2005, 43, 1166.
31. Vera, M.; Admetlla, M.; Rodríguez-Galán, A.; Puiggalí, J. Polym Degrad Stab 2005, 89, 21.
32. Yang, K. K.; Wang, X. L.; Wang, Y. Z.; Wu, B.; Jin, Y. D.; Yang, B. Eur Polym J 2003, 39, 1567.
33. Vera, M.; Franco, L.; Puiggalí, J. Macromol Chem Phys 2004, 205, 1782.
34. Botines, E.; Franco, L.; Ramis, X.; Puiggalí, J. J Polym Sci Part A: Polym Chem 2006, 44, 1199.
35. Vyazovkin, S.; Dollimore, D. J Chem Inf Comput Sci 1996, 36, 42.
36. Coats, A. W.; Redfern, J. P. Nature 1964, 201, 68.
37. Kissinger, H. E. Anal Chem 1957, 29, 1702.
38. Friedman, H. J Polym Sci Part C: Polym Symp 1964, 6, 183.
39. Ozawa, T. Bull Chem Soc Jpn 1965, 38, 1881.
40. Flynn, J. H.; Wall, L. A. J Res Natl Bur Stand Sect A 1966, 70, 487.
41. Mianowski, A. J Therm Anal Cal 2003, 74, 953.
42. Lesnikovich, A. I.; Levchik, S. V. J Therm Anal 1983, 27, 89.
43. Lesnikovich, A. I.; Levchik, S. V. J Therm Anal 1985, 30, 677.
44. Minying, L.; Lijun, G.; Qingxiang, Z.; Yudong, W.; Xiaojuan, Y.; Shaokui, C. Chem J Internet 2003, 5, 43.
45. Vert, M.; Mauduit, J.; Li, S. M. Biomaterials 1994, 15, 1209.